Dynamics of the Reaction of O(^{3}P) Atoms with Alkylthiol Self-assembled Monolayers†

Carla Waring,‡ Paul A. J. Bagot,‡ Minna T. Räisänen,§ Matthew L. Costen,‡ and Kenneth G. McKendrick*,‡

School of Engineering and Physical Sciences, Heriot-Watt University, Edinburgh EH14 4AS, U.K. and School of Chemistry, University of St. Andrews, St. Andrews, Fife KY16 9ST, U.K.

Received: December 12, 2008; Revised Manuscript Received: February 20, 2009

We have studied the dynamics of the reactions of O(^{3}P) atoms with alkylthiol self-assembled monolayers (SAMs). Superthermal O(^{3}P) atoms, with a fairly broad distribution of laboratory-frame kinetic energies (mean = 16 kJ mol^{-1}, fwhm = 26 kJ mol^{-1}), were generated by 355 nm photolysis of NO_2 introduced at a low pressure above the SAM surface. Nascent OH $v' = 0$ products were detected by laser-induced fluorescence. SAMs of two different alkyl chain lengths, C_6 and C_{18}, were studied. The existence of SAM layers, and their robustness under our experimental conditions during the relevant measurement period, were confirmed by scanning-tunneling microscopy (STM). Reaction at the SAM surface was verified as the authentic source of the hydroxyl radicals using a perdeuterated C_6D_{13}-SAM sample. The OH appearance profiles as a function of photolysis-probe delay, and the rotational-state distributions at their peaks, were compared with those of liquid squalane ($C_{30}H_{62}$, 2,6,10,15,19,23-hexamethyltetracosane). The reactivity of the SAMs and of squalane was found to be comparable. We conclude that the O(^{3}P) atoms must be able to access the more reactive secondary hydrogen atoms along the alkyl chains of the SAMs. We find no perceptible differences in reactivity or product energy disposal between the two SAM chain lengths. Both produce a substantial fraction of the OH with relatively high velocities, which must result from direct, impulsive reaction. There is also a slower component, with velocities consistent with a thermal, trapping-desorption mechanism. The proportion of this component appears to be lower for SAMs than for squalane. This would be compatible with the expected greater smoothness of the SAM surface at the molecular scale. We find little evidence for significant rotational excitation of the OH products, although the details of any correlation between translational and rotational energy release require further investigation. We compare our results with the limited available prior theoretical modeling of O(^{3}P) + SAM systems.

Introduction

A detailed knowledge of the dynamics of reactions between gases and condensed phases is fundamental to the understanding of interfacial chemistry. Collisions of gases with solid surfaces have been extensively investigated at a detailed dynamical level. However, their interactions with "softer" liquid surfaces have been much less explored. In this work, we address the dynamics of reactive collisions with self-assembled monolayers (SAMs), which bridge the gap between more fully characterized solid and relatively disordered liquid surfaces.

SAMs are formed by the spontaneous chemisorption of amphiphillic molecules onto a solid substrate. Alkylthiols adsorbed onto Au(111) substrates have been particularly well studied.[1] The functionality and structure of the interface can be tailored to design, making SAMs ideal systems for a wide range of applications including microelectronics, lubrication, and wettability control and in the design of biotechnological devices.[2] In the context of the current work, they are particularly interesting through their potential to create well-defined, partially ordered surfaces which mimic the supramolecular structure that may be spontaneously present at the surfaces of liquids.

Although the dynamics of reactions at SAMs surfaces remain almost completely unexplored experimentally, there have been a limited number of previous studies of their kinetics. Naaman and co-workers[3,4] have examined the oxidation of methyl-terminated SAMs by O(^{3}P) atoms. The surfaces investigated included methyl-terminated $C_{18}H_{37}$ (OTS) and CH_3 (MTS), both adsorbed through a covalent silane attachment to glass or polished quartz substrates. The destruction of the monolayer was followed using surface-specific IR absorption and X-ray photoelectron (XPS) spectroscopies. The temperature dependence yielded activation energies, stimulating speculation on possible reaction mechanisms, including the degree of penetrability of the surface. This aspect was investigated more directly in related work by Jacobs and co-workers on etching of site-selectively deuterated SAMs by O^+ ions at much higher collision energies (5−40 eV).[5−7] Fairbrother and co-workers have also examined the destruction of alkyl, fluorinated, and X-ray-modified SAMs by a thermalized mixture of atomic and molecular oxygen (O(^{3}P)/O_2) generated by an electric discharge in O_2. The integrity of the structures was again monitored by XPS.[8,9] The secondary reactions with O_2 of the alkyl radical formed through the initial abstraction of a hydrogen atom by O(^{3}P) were investigated. A range of oxygen-containing functional groups were formed initially, including alcohol, carbonyl, and carboxylic acids. Longer exposure times led to the formation of Au_2O_3 and sulfonate groups (RSO_3), with the removal of the monolayer following pseudo-first-order kinetics.

In contrast to reactive processes at the gas−SAM interface, the dynamics of inelastic collisions between (mostly) closed-shell species and SAMs have been more widely investigated.

† Part of the George C. Schatz Festschrift.

* Corresponding author: k.g.mckendrick@hw.ac.uk.
§ University of St. Andrews.
‡ Heriot-Watt University.

10.1021/jp8109868 CCC: $40.75
Published on Web 03/23/2009

The first such experiment was carried out by Naaman and co-workers[10] using molecular beams of He, Ar, NO, and O_2 from alkyl and fluorinated SAMs and time-of-flight mass spectrometry (TOF-MS) to detect the scattered species. Subsequent work by Siebener and co-workers[11−15] and, most comprehensively, by Morris and co-workers[16−26] has investigated the effects of varying the identity of the impinging gas, impact angle, final angle, initial energy, monolayer temperature, SAM terminal group, alkyl chain length, and metal substrate (hence, surface density). This has led to a wealth of information on factors affecting energy transfer at the gas−SAM interface. This approach builds on an extensive body of closely related work by Nathanson and co-workers on inelastic scattering at the gas−liquid interface.[27,28] Some concepts common throughout gas-condensed phase collision dynamics have been established. It is found very widely that product translational energy distributions are bimodal. This can be explained, at least to a first approximation, as resulting from two extremes in scattering mechanism: a faster "impulsively scattered" (IS) component, in which the projectile scatters directly, experiencing one, or at most a few, encounters with the surface, and a slower "trapping desorption" (TD) component, consistent with the gas species being trapped on the surface and undergoing multiple collisions before thermally desorbing.

The experimental studies on inelastic scattering from SAMs have been complemented by a number of theoretical investigations, greatly enhancing the mechanistic interpretation.[13−15,19,22,25,29−36] The notable gap that exists in experimental studies of reactive dynamics at SAM surfaces does not apply equally to theoretical investigations. In fact, the relative order that is present in SAM surfaces has made them attractive proxies as an alternative to the more challenging treatment of reactions on more complex liquid structures.[37] The first preliminary trajectory study of reactions of O(^{3}P) with a SAM layer was carried out by Hase and co-workers,[30] at a range of collision energies spanning thermal to hyperthermal. The same group went on to study the inelastic scattering dynamics in more detail,[33] extending their related work on inelastic scattering of closed shell species.[13,14,24,26,29,31,32,34,38] The reactive dynamics at hyperthermal energies (5 eV) have also been investigated by Schatz and Troya,[39] motivated in part by the oxidation of hydrocarbon polymers by O(^{3}P) on the outer surfaces of spacecraft in low earth orbit (LEO).[40−42] Both sets of dynamical scattering calculations adopted mixed "QM/MM" approaches, in which the O atom and outer parts of the alkyl chain are treated quantum mechanically while the rest of the alkyl chain, sulfur atom, and gold atoms are treated by molecular mechanics.

Our current experiments are a natural extension of our related work on the dynamics of the reactions of photolytically generated O(^{3}P) atoms at the surfaces of a range of liquid hydrocarbons.[43−49] We use laser-induced fluorescence (LIF) spectroscopy to detect the hydroxyl radicals formed at the liquid surface, yielding information on their translational and internal state distributions. This is a development of the earlier work of McCaffery, who was the first to use LIF spectroscopy to detect I_2 inelastically scattered from a range of liquid surfaces.[50−52] In subsequent related work, Nesbitt and co-workers have used IR absorption spectroscopy to study both inelastic scattering of CO_2[53−56] and the reactions of F atoms[57] with liquid surfaces.

Most of our work on O(^{3}P) + hydrocarbons has concentrated on the "benchmark" branched hydrocarbon molecule, squalane ($C_{30}H_{62}$, 2,6,10,15,19,23-hexamethyltetracosane). The time-dependent appearance profiles could be deconvoluted into a distinct pair of velocity distributions, assignable to the limiting IS and TD types noted above. This reproduced the more highly resolved bimodal velocity and angular distributions obtained earlier by Minton and co-workers.[58−61] They used complementary molecular-beam scattering methods that were an evolution of Nathanson's approach to inelastic scattering.[27,28] With the added state-selectivity of LIF detection, we have been able to extract internal state distributions for both of these components.[46] The OH rotational distributions measured at early delay times were consistent with the OH being formed by a direct abstraction reaction in which the remainder of the surface is essentially a spectator. Those at longer delay times were found to be modified to an extent dependent on the liquid temperature. This is consistent with some of the OH having resided on the liquid surface sufficiently long to be translationally and rotationally (but not vibrationally) thermalized. This conclusion was corroborated by our subsequent work on the inelastic scattering of OH radicals themselves from liquid surfaces.[62] We have also gone on to study the relative reactivity of O(^{3}P) and OH-product energy partitioning for a range of different hydrocarbons. It is believed on the basis of molecular dynamics (MD) simulations[37,45,49,63−65] that for squalane all three C−H bond types (primary, secondary, and tertiary) are available for abstraction. The observed lower reactivity of linear hydrocarbons[49] has, supported by independent experimental[66−74] and theoretical evidence[68,75−77] of surface ordering effects, been inferred to be the result of the interface being dominated by less reactive, primary end groups.

It is this type of mechanistic question that we begin to address in the current work through the alternative route provided by the surface ordering of SAM layers. We report here the first dynamical experimental investigation of a reaction at the surface of a SAM. Specifically, we have studied the reaction between superthermal O(^{3}P) atoms and linear alkylthiol SAMs of two different chain lengths. We examine what effect the ordering of the SAM layer has on the reactivity with O(^{3}P) and the nascent internal and translational energy disposal in the product OH, in comparison to liquid squalane.

Experimental Methods

SAM specimens were prepared by immersing flame-annealed Au(111)-coated mica slides (PHASIS-SARL, 25 × 25 mm) in solutions containing the relevant thiol molecules. The thiols (all ≥98% purity) used were $C_6H_{13}SH$, $C_{18}H_{37}SH$ (Sigma-Aldrich), and the species $C_6D_{13}SH$ (CDN isotopes) with a perdeuterated alkyl chain. Solutions were prepared at millimolar concentrations in ethanol or tetrahydrofuran (THF), depending on the solubility of the thiol. Slides were held in solution for a minimum of 6 h, although normally overnight, before being removed from solution. They were rinsed with ethanol, dried with N_2 (research grade), and used immediately. The SAMs were characterized by scanning-tunneling microscopy (STM), recorded in constant current mode under ambient pressure with a PicoPlus (Molecular Imaging) instrument. Tips were shaped by mechanically cutting a Pt/Ir (80:20) wire (0.25 mm diameter, Advent Research Materials Ltd.). Bias and currents were typically 520 mV (tip positive) and 30 pA.

The experimental setup used to study the reaction of oxygen atoms with the SAM specimens was an adaptation of that used previously for gas−liquid reactions and inelastic scattering.[43,44,46−49,62] A schematic of the revised apparatus is shown in Figure 1. It is a dual-chamber design, with the subsidiary, turbopumped chamber allowing SAM specimens to be stored rapidly under vacuum on removal from their solutions.

When a SAM specimen was ready to be used, it was moved to the main reaction chamber using the magnetic transfer arm,

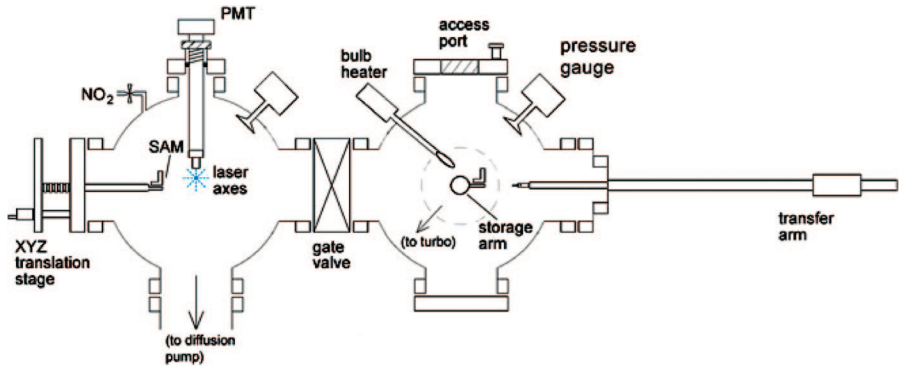

Figure 1. Schematic of the vacuum system used to study reactions of $O(^3P)$ with SAMs.

where it was located in place on an XYZ translation stage. This enabled the sample to be held at a precisely controlled distance (typically 4 mm) from the central laser axis, which was determined accurately prior to the experiments by a series of calibration tests. All results in the current work were obtained with the SAM sample at room temperature (nominally 296 K).

To allow comparison with reaction of $O(^3P)$ atoms with a liquid squalane ($C_{30}H_{62}$, 2,6,10,15,19,23-hexamethyltetracosane) surface, the setup was returned to its original configuration, which has been fully described in an earlier publication.[44] The SAM stage was replaced by a stainless-steel wheel of 50 mm diameter. This was mounted on an axle, rotating at 0.5 Hz through the hydrocarbon liquid of interest contained in a copper bath, which in the current work remained at room temperature. This arrangement provided a continuously refreshed liquid squalane surface. Squalane was supplied by Sigma-Aldrich (99%) and used without further purification.

Regardless of the nature of the surface, $O(^3P)$ atoms were generated by photolyzing a carefully controlled pressure (nominally 1 mTorr) of NO_2 (BOC, 98.3%). Before admission to the vacuum chamber, sufficient NO_2 was purified by three cycles of freeze−pump−thawing to remove any noncondensable contaminants. Photolysis of the NO_2 was achieved using the third harmonic of a Nd:YAG laser (Continuum Surelite II-10), supplying 355 nm light pulses of width 4−6 ns at 10 Hz. The laser energy was maintained at a constant value of around 70 mJ per pulse, measured upon entry to the vacuum chamber. The photolysis beam counter-propagated the probe beam, passing at the same carefully controlled distance from the surface. The spatial distribution of the $O(^3P)$ produced in this manner is described by an anisotropy parameter, $\beta = +0.7$.[78] The photolysis laser was horizontally polarized, so roughly half of the $O(^3P)$ was directed toward the SAM or liquid surface. The collision energy of the $O(^3P)$ atoms is broadly distributed around an average value of 15.8 kJ mol^{-1} (with a fwhm of 26 kJ mol^{-1}) in the laboratory frame, corresponding to an average speed of 1340 ms^{-1}.[78]

When the $O(^3P)$ atoms impact on the SAM/liquid surface, some of them extract hydrogen (or deuterium) atoms, generating OH (or OD) $X^2\Pi$ radicals. A fraction of these escape from the surface and are detected by LIF. In the current work we have only attempted to detect vibrational ground-state OH or OD on their respective $A^2\Sigma^+$-$X^2\Pi$ (1,0) bands using a Nd:YAG (Continuum Surelite II-10) pumped dye laser (Sirah Cobra Stretch). This supplied ca. 1 mJ, 4−6 ns pulses, again measured at the entrance to the vacuum chamber. The returning *A*-*X* fluorescence was collected by a liquid light guide (Ultrafine Technology, Ltd.) mounted 2 cm directly above the common laser axis. The fluorescence passed through custom interference filters before being converted into a signal by a photomultiplier tube (PMT, Electron Tubes Ltd.). This signal was in turn digitized and passed to a PC, which collected data and controlled the wavelength and timing of the lasers using custom-written LabVIEW programs.

As explained fully in the following sections, experiments could be split into two basic types. The first were *appearance profiles*, acquired by varying the time delay between the photolysis and probe lasers to gain information on the translational energy of the escaping OH/OD species in a particular rotational (and fine-structure and Λ-doublet) state of $v' = 0$. The second were LIF *excitation spectra*, acquired by scanning the wavelength of the probe laser at a fixed photolysis-probe delay. These spectra yield information on the product rotational state distributions. To extract nascent populations, the spectra were compared with those from a known "thermalized" distribution, as we have described in our previous work.[44] The thermal spectra were obtained by photolyzing the precursor molecule HONO (or DONO for OD radicals) at 355 nm. Gaseous HONO was prepared by adding NO_2 (containing some NO impurity) to a flask containing a few milliliters of H_2O (or D_2O-Sigma Aldrich, 99% purity) and then leaving the mixture to stand overnight. This yields HONO according to the following equilibrium:

$$NO_{2(g)} + NO_{(g)} + H_2O_{(l)} \rightleftharpoons 2HONO_{(g)} \qquad (1)$$

The resulting gaseous mixture was admitted to the chamber at the desired total pressure (nominally 1 mTorr) using a needle valve. To ensure rotational thermalization of the OH or OD molecules, 0.5 Torr of high-purity N_2 was added to the chamber. The excitation spectrum was recorded at a photolysis-probe delay of 10 μs, corresponding to approximately 50 collisions based on a typical gas-kinetic collision rate constant of 10^7 Torr^{-1} s^{-1}.

Results

Verification of Source of OH/OD Radicals. Clearly, it was essential to ensure that the hydroxyl radicals detected by LIF were the product of $O(^3P)$ reaction at the SAM surface and that this surface remained effectively unmodified during the measurement of OH product attributes.

The first requirement was met conclusively through measurements on perdeuterated C_6D_{13}−SAMs. These were deposited on Au substrates from a solution of $C_6D_{13}SH$, as described above. Following rapid transfer to the vacuum system, unmistakable OD LIF signals were detected when NO_2 was photolyzed above the SAM surface. The appearance profiles confirm that

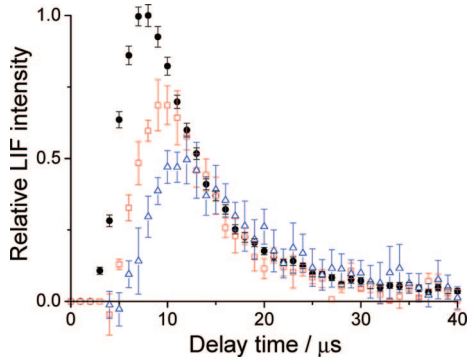

Figure 2. Measured appearance of the OD *A-X* (1,0) $Q_1(1)$ LIF signal as a function of photolysis-probe delay time from a C_6D_{13}−SAM. Nominal probe-laser beam to SAM distance of 4 mm (black filled circles), 5 mm (red open squares), and 6 mm (blue open triangles). $p(NO_2)$ ~1 mTorr.

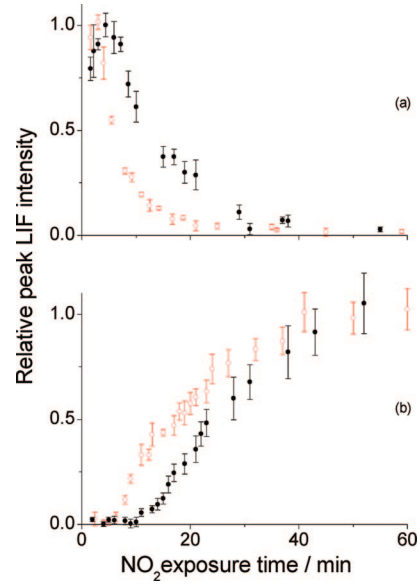

Figure 3. Intensity of LIF signals for (a) OD and (b) OH from reaction of O(^{3}P) with a C_6D_{13}−SAM as a function of NO_2 exposure time. NO_2 pressures of 2 mTorr (black filled circles) and 6 mTorr (red open circles). Each point represents the peak height (with background subtracted) from a measured appearance profile. Data were recorded on the OD/OH *A-X* (1,0) $Q_1(1)$ line at a probe laser-SAM distance of 4 mm. Relative intensities for OH and OD at both pressures have been arbitrarily normalized to the peak signals at long and short exposure times, respectively.

reaction at the SAM surface is definitely the source of these OD radicals, so it is not necessary to rely on (actually very secure) indirect arguments that there are no plausible gas-phase sources of OD. Typical profiles are shown in Figure 2. They are qualitatively similar to those in our earlier work on liquid surfaces.[43−49] They consist of a characteristic "dead time" after the photolysis pulse, followed by a returning wave of OD. They show the variations expected with the distance between the common laser axis and the surface. The peak arrival times are consistent with the known average velocity of the O(^{3}P) atoms and reasonable assumptions about the recoil velocities of the OD products. The magnitude of the signal also drops, as expected, for simple geometric reasons.

We investigated the second requirement on the persistence of the SAM surface in several ways. There is, by the nature of our experimental method, some chemical modification through the abstraction of H (or D) atoms by the O(^{3}P). For liquid samples, continual refreshment of the surface is ensured by the rotation of the wheel. However, for the SAM specimens the surface is necessarily static. We have made an order-of-magnitude estimate of the rate of erosion based on the known absorption cross section and near unit quantum yield for photolysis of NO_2 at 335 nm, the typical pressure of 1 mTorr, the known photolysis laser fluence, an estimate of the fraction of the O(^{3}P) that hits the surface, and the area that it doses. This calculation indicates that, on the (deliberately worst-case) assumption that every O(^{3}P) that hits the surface reacts, the time to extract one hydrogen from each terminal CH_3 group would be around 8 min. The true absolute reactivity of the O(^{3}P) with an alkyl SAM is, of course, unknown. However, it is likely, on the basis either of related measurements on liquid surfaces where inelastic scattering is known to be the major channel[58,60] or a priori arguments based on gas-phase activation energies and Arrhenius factors,[79,80] to be much less than unity. We therefore believe this is not the practical limiting factor on the useful lifetime of the SAMs under our conditions.

Particularly for the shorter chain (C_6) SAMs, some instability of the SAM surface over extended periods is expected, depending on the conditions.[81,82] In our experiments, we must necessarily introduce the precursor. We established empirically that it was this which set the practical limits on the length of the safe working window in our experiments. The magnitude of the OD signal was found to decay over a period of ca. 1 h. This loss only happened when the NO_2 was flowing and was independent of the presence of the photolysis laser. In addition, there was concomitant growth of a spurious OH signal. The kinetics of these changes were nonlinear, with an empirical dependence on NO_2 pressure that is illustrated in Figure 3. There was an initial period from first exposure to the NO_2 in which the loss of OD and the growth of OH were effectively negligible. The length of this period decreased with pressure. For our lower, standard operating pressure of 1 mTorr in the measurements below, it was found conservatively to exceed 10 min.

We examined the corresponding changes in the microscopic state of the SAM surfaces using STM. Large-scale images (250 nm × 250 nm) of a freshly prepared SAM (Figure 4a,b) show structures typical of thiolalkyl SAM layers prepared at room temperature. A separate SAM sample which had been exposed to NO_2 (and O(^{3}P)) in the reaction chamber for 10 min had essentially equivalent characteristics (Figures 5a,b). The most distinctive features are gold vacancy islands of 0.24 nm depth which are characteristic of alkylthiol SAMs. On both surfaces a full monolayer is observed with relatively low crystalinity and small domains. These observations support our underlying assumption that what we measure in LIF experiments is representative of the majority of alkyl chains which lie within the well-ordered regions of the surface. The domain boundaries make up only a small proportion of the total number of SAM molecules, which is the basis of previous measurements of this type, for example by Jacobs.[7] The thiol molecules are in an upright position, with a known average tilt angle of 30 degrees relative to the surface normal, and are densely packed in a hexagonal arrangement.[83] High-resolution images (Figures 4b and 5b) show that there are small areas of high crystalinity.

In marked contrast, a large-scale (250 nm × 250 nm) STM image (Figure 6a) of a C_6H_{13}−SAM that has been exposed to NO_2 for 1 h clearly shows that the SAM structure is distinctly different and is partially damaged. There are smooth and rough areas on the surface, and the gold vacancy islands are not as pronounced. Small-scale STM images (Figure 6b) reveal that the smooth areas consist of a striped structure of thiol molecules

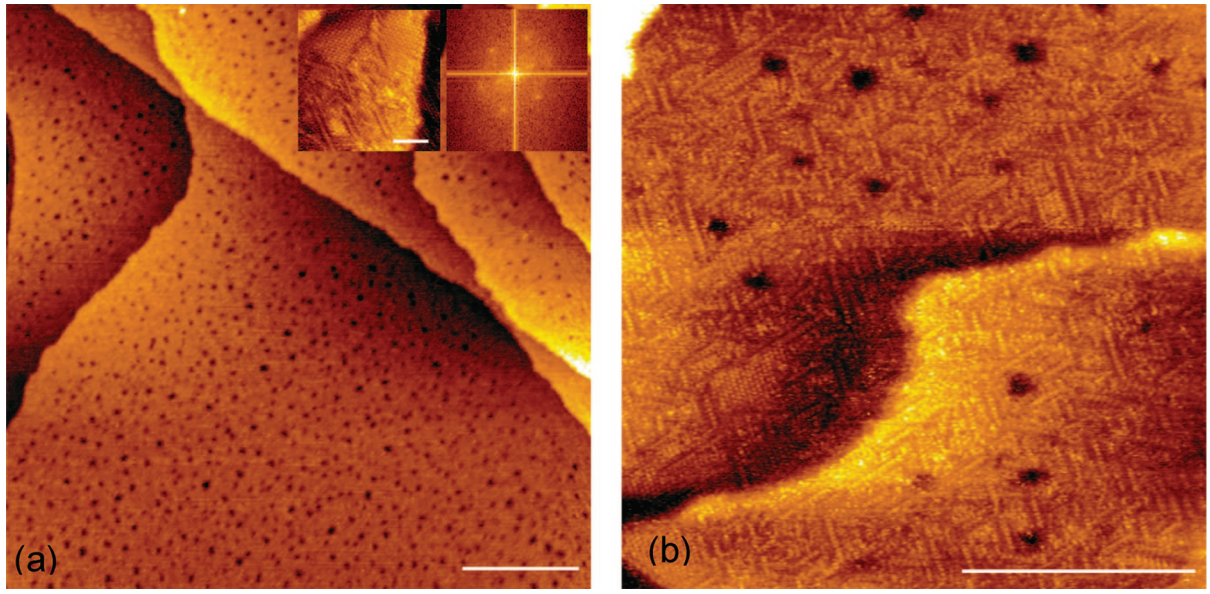

Figure 4. STM images of a freshly prepared C_6H_{13}−SAM: (a) large-scale image (250 nm × 250 nm) showing 0.24 nm deep gold vacancy islands (scale bar 50 nm) and fast-Fourier transform of high-resolution image inset (scale bar 5 nm), indicating hexagonal packing; (b) high-resolution image (50 nm × 50 nm) showing densely packed hexagonal arrangement of molecules in those areas with high crystallinity (scale bar 20 nm).

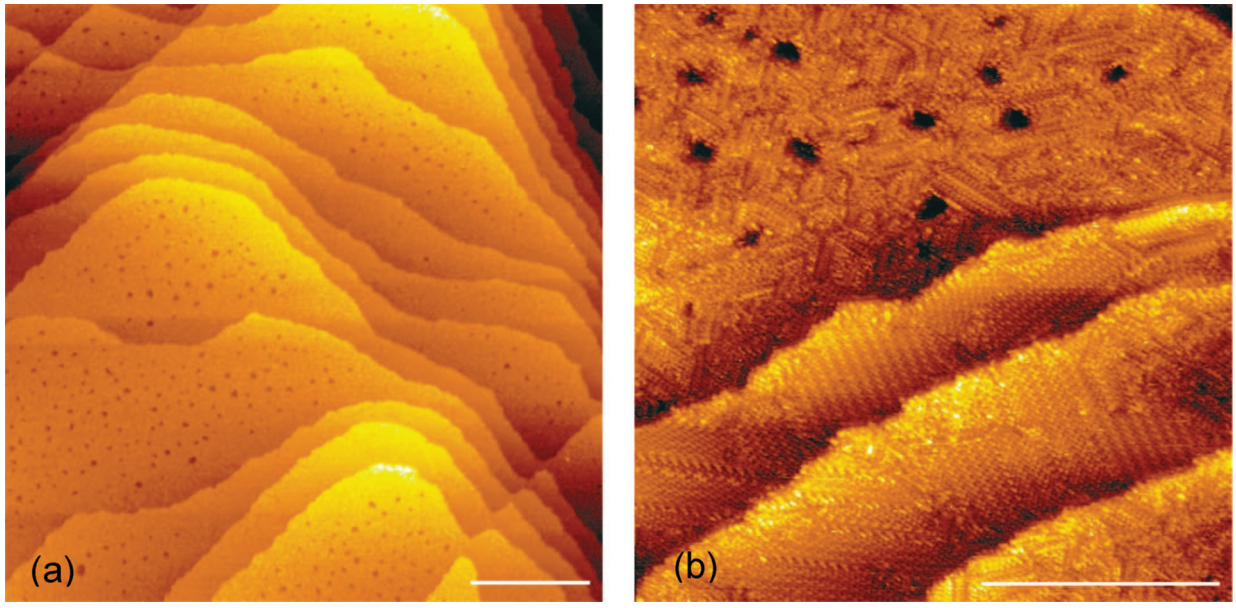

Figure 5. STM images of a C_6H_{13}−SAM after 10 min in reaction chamber in the presence of NO_2: (a) large scale image (250 nm × 250 nm) showing characteristic gold vacancy islands (scale bar 50 nm); (b) high-resolution image (50 nm × 50 nm) showing densely packed upright chains in a hexagonal arrangement in an area of high crystallinity (scale bar 20 nm).

with an inter-row periodicity of 1.3 nm. In this phase, the remaining molecules are lying flat on the surface,[84] consistent with a SAM which has been substantially eroded.

These changes in the STM images were corroborated by XPS measurements (see the Supporting Information). The XPS spectrum of a fresh SAM layer contained elemental peaks in the ratios expected.[85] This spectrum was also invariant over a 2-h time period at the base pressure of $\sim 1 \times 10^{-7}$ mbar or following exposure to 1 mTorr of pure N_2. However, extended exposure to 1 mTorr of NO_2 resulted in substantial changes to the XPS spectrum, which became dominated by the C 1s peak rather than the Au 4f. This suggests that the H-containing species that we presume opportunistically adsorbs to the damaged SAM layer at long exposure times, explaining the growth of the spurious OH signal from the per-deuterated SAM, may be a hydrocarbon impurity.

Regardless of the precise mechanism of the erosion and subsequent contamination, we avoided their effects by ensuring that all LIF data presented below are from specimens, for both deuterated and normal SAMs, exposed to NO_2 for less than 10 min. Within this period, all the SAM samples gave reproducible LIF signals when all other parameters were carefully maintained constant (especially laser energies, gas pressure, and distance of the wheel/SAM specimen from the laser axis). This naturally makes the experiments we report here considerably more challenging than our previous work on liquids,[43−49,62] where much longer signal acquisition times were possible.

Appearance Profiles. Typical appearance profiles for OD $v' = 0$ measured on the $Q_1(1)$ line from the C_6D_{13}−SAM have already been shown in Figure 2. We carried out a more systematic investigation for the normal hydrogen SAMs, collecting profiles on each of the $Q_1(1)$ and $R_1(5)$ OH lines, for

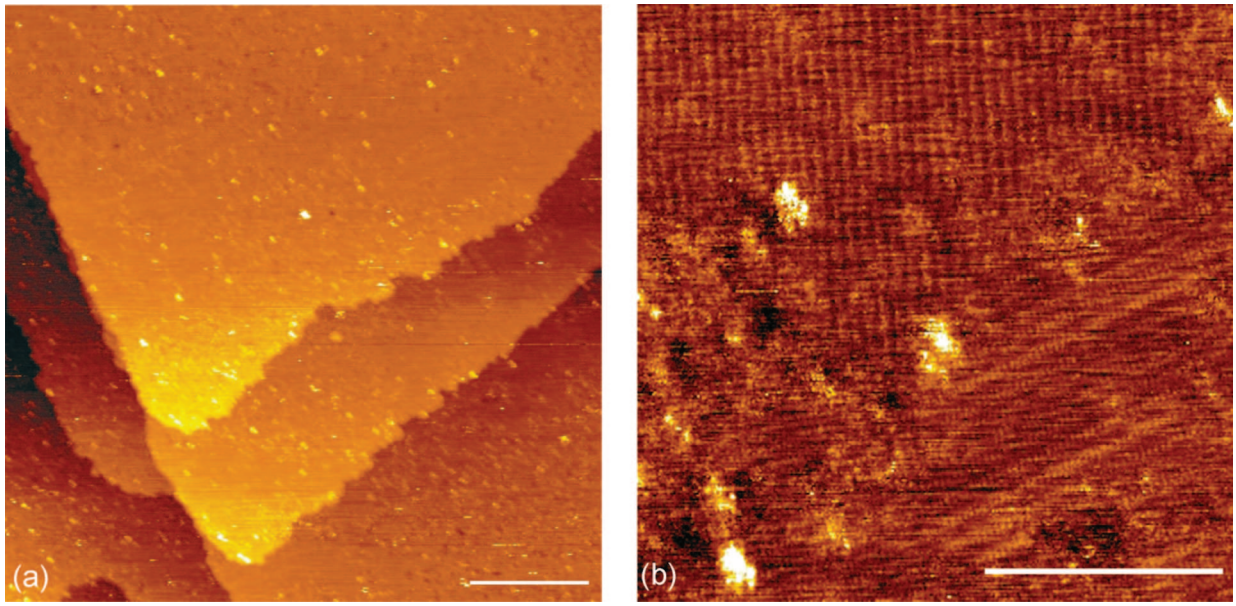

Figure 6. STM images of a C_6H_{13}−SAM after 60 min in the reaction chamber in the presence of NO_2: (a) large-scale image (250 nm × 250 nm) showing less pronounced gold vacancy islands (scale bar 50 nm); (b) high-resolution image (50 nm × 50 nm) showing the striped structure with an inter-row periodicity of 1.3 nm (scale bar 20 nm).

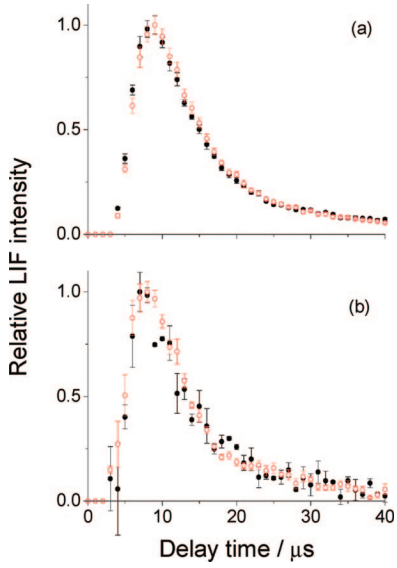

Figure 7. Measured appearance profiles of OH ($v' = 0$) recorded on the (a) $Q_1(1)$ and (b) $R_1(5)$ transitions of the *A*-*X* (1,0) band from a C_6H_{13}−SAM (black filled circles) and a $C_{18}H_{37}$−SAM (red open circles). The relative signal heights from the two SAM types are shown as measured and have not been separately normalized. Probe laser−SAM distance = 4 mm; $p(NO_2)$ ~1 mTorr.

both alkyl chain lengths C_6H_{13}−SAM and $C_{18}H_{37}$−SAM. These results are collected in Figure 7. The profiles are averages of ~12 individual measurements on separate SAM samples, replaced as explained above after less than 10 min exposure to NO_2. We endeavored to maintain very careful control of the laser axis−SAM surface distance when changing samples.

It is clear that for both rotational lines the profiles for the two SAM chain lengths are very similar. Any differences lie within the mutual error bars. Careful comparison of parts a and b of Figure 7 reveals some possible minor systematic differences between the two rotational lines. For both SAM chain lengths, the $R_1(5)$ profile peaks slightly earlier than $Q_1(1)$. However, these differences are marginally significant within the signal-to-noise ratio (which is naturally smaller for the weaker $R_1(5)$ line).

As noted above, we also reconfigured the chamber to allow direct comparison with the appearance profiles for O(^{3}P) reaction with the previously most heavily studied[43−46,48] liquid, squalane. We took particular care to ensure that distance from the laser axis to the surface of the liquid wheel was the same as that for the SAMs. We do not attempt to report quantitative relative signal sizes from the two samples because of the considerable delay between measurements unavoidably introduced by reconfiguration of the chamber. Nevertheless, at a qualitative level, the yields of OH were found to be quite similar. The raw, uncorrected OH signals from squalane were only slightly larger. We are, however, able to make reliable comparisons of the normalized profiles. Figure 8a shows the $Q_1(1)$ profiles for the two SAMs alongside that for squalane. There are now obvious differences between the SAMs and squalane that significantly exceed the statistical uncertainties (as represented by the error bars). The squalane profile has a slightly later peak and a broader shoulder to later times, presumed to correspond to slower-moving OH.

LIF Excitation Spectra. We have recorded nascent LIF excitation spectra from the SAM surfaces at the single photolysis-probe delay of 8 μs, close to the peak of the profiles in Figure 7. A representative spectrum in the region of the Q_1 branch is shown in Figure 9b. As in our previous work,[43−49,62] the spectra were analyzed by constructing Boltzmann plots from which effective temperatures could be extracted. The relative intensities of lines in the nascent spectrum can be seen to be close to those in the thermal calibration spectrum in Figure 9a. This naturally resulted in a fitted temperature that was not far from ambient. Repeated independent measurements on the Q_1- and R_1-branches for OH, and the Q_1 branch for OD (for which the R_1 branch is accidentally too blended to be used reliably), gave the average temperatures in Table 1.

Discussion

Our results unambiguously provide the first direct experimental evidence that alkylthiol−SAM layers undergo an elementary reaction with superthermal O(^{3}P) atoms to produce OH. We find no significant differences in either reactivity or

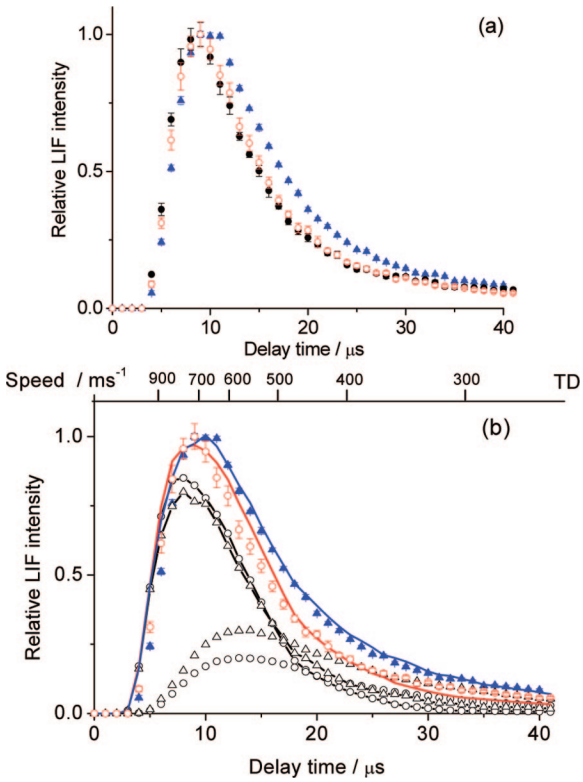

Figure 8. (a) Peak-normalized appearance profiles of OH ($v' = 0$) recorded on the $Q_1(1)$ transition of the *A-X* (1,0) band from a C_6H_{13}−SAM (black filled circles), $C_{18}H_{37}$−SAM (red open circles), and liquid squalane (blue filled triangles). Background signals due to the probe and photolysis lasers have been subtracted. Probe laser-surface distance = 4 mm; $p(NO_2)$ ~1 mTorr. (b) Measured profiles (symbols as in (a)) for the $C_{18}H_{37}$−SAM and squalane. Superimposed are the MC-model predictions of the direct (IS) component from a SAM (black open circles with black line) and liquid surface (black open triangles and black line); MC-model predictions of a thermal (TD) component from a SAM (black open circles) and liquid surface (black open triangles); weighted sums of IS and TD predicted profiles from a SAM (~80:20, red solid line) and from a liquid (~70:30, blue solid line). The average speeds of the predicted TD component are indicated, as discussed in the text.

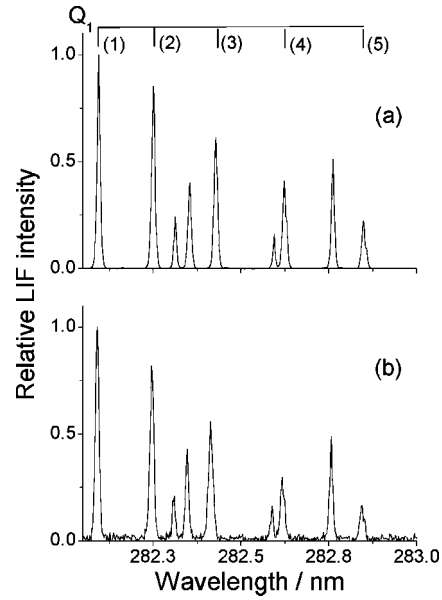

Figure 9. Representative OH *A-X* (1,0) excitation spectra. (a) Thermal spectrum recorded at a photolysis-probe laser delay of 10 μs, $p(NO_2)$ ~1 mTorr and $p(N_2)$ ~0.5 Torr. Q_1-branch line positions are indicated. (b) Nascent spectrum recorded at a photolysis-probe laser delay of 8 μs, probe laser−SAM (C_6H_{13}−SAM) distance = 4 mm $p(NO_2)$ ~1 mTorr.

TABLE 1: Rotational Temperatures of Nascent OH/OD ($v' = 0$) Formed by Reaction of (O^3P) Atoms and Perdeuterated and Fully Hydrogenated Alkylthiol−SAMs, Measured at a Photolysis-Probe Delay of 8 μs

T_{rot}/K	C_6D_{13}−SAM	C_6H_{13}−SAM	$C_{18}H_{37}$−SAM
R_1 branch average		283 ± 5	286 ± 2
Q_1 branch average	320 ± 8	280 ± 4	287 ± 7
weighted average	**320 ± 8**	**281 ± 3**	**286 ± 4**

OH product translational or rotational distributions between SAMs with alkyl chain lengths of C_6 and C_{18}. Although as yet not precisely quantified, we find that the reactivity is also not greatly different from that of the "benchmark" liquid, squalane.[43−48]

These observations suggest that the $O(^3P)$ must be able to penetrate beyond the terminal $-CH_3$ groups of the alkyl chains. It is very well-known from the gas phase[79,80] that the reactivity of H−C bonds with $O(^3P)$ is inversely correlated with the H−C bond strength and, hence, increases markedly from primary to tertiary. It has also been established through realistic MD simulations[37,45,49] that the surface of squalane is only moderately ordered. There is only a modest nonstatistical preference for $-CH_3$ groups to be present in the outermost layer, with the more reactive secondary and tertiary groups also significantly exposed. We therefore think it quite unlikely that the reactivity of the SAMs would approximately match that of squalane unless the $O(^3P)$ could access the more reactive secondary H−C bonds along the alkyl chains.

This conclusion is consistent with the kinetic results of Naaman and co-workers[3,4] using thermal $O(^3P)$ atoms, where the reactivity of a related long-chain (C_{18}) self-assembled layer was found to be greater than that of a simple methyl layer. This was also ascribed to penetration of the C_{18} chains to access the more reactive secondary hydrogens. It may also be compared with the predictions of theoretical modeling of the scattering of $O(^3P)$ from SAM layers.[30,33,39] In the original work of Hase and co-workers,[30] the initial conditions were chosen in such a way that reaction was effectively restricted to the terminal $-CH_3$ group. Although Troya and Schatz[39] also did not examine a fully randomized initial distribution, they did include a sufficient range of impact parameters and angles to identify that O atoms are indeed able to extract H from more than just the terminal carbons, at least at the high initial energy of 5 eV. Abstraction is seen from at least as deep as C_4. The proportions from different carbons vary very strongly, as would be expected, with the polar and azimuthal angles relative to the orientation of the alkyl chains. This affects the group most likely to be struck on the first encounter and the subsequent depth of penetration of the trajectory into the layer. We know in our experiments that the photolytic production results in a broad range of polar angles. We assume that the large number of domains across the SAM surface, revealed by the STM images in Figure 5b, results in an essentially random distribution of azimuthal angles. For at least some azimuthal and polar angles, Troya and Schatz's calculations[39] indicate that the secondary C_2 units are exposed to direct attack. The more extensive range of initial geometries in Hase and co-workers' later work[33] on inelastic scattering of O atoms confirms that, even at lower collision energies, a significant fraction of trajectories enter the channels between the alkyl chains, by implication accessing the more reactive secondary hydrogens.

Further experimental insight into the microscopic mechanism may be gained from the observed OH product energy disposal. The clearest aspect of our results is that a substantial fraction of the OH is translationally hot. To demonstrate this, we have included in Figure 8b two sets of simulated appearance profiles (shown with weightings that we explain shortly below), based on the binary separation into limiting IS and TD components discussed in the Introduction. The profiles were generated by a Monte Carlo method similar to that which we have described previously.[62] In essence, the procedure involves sampling at random an initial location of the photolyzed NO_2 molecule within the photolysis laser beam volume. An $O(^3P)$ velocity is then selected from the known speed and angular distributions for 355 nm photolysis of NO_2.[78] A subset of these trajectories strike the SAM or liquid surface. The recoiling OH velocities of OH starting from each of these points are then sampled from distributions appropriate to either direct impulsive scattering (IS) or thermal desorption (TD), respectively. The more straightforward of these is for the TD component. The speeds are chosen from a Maxwell−Boltzmann distribution at the surface temperature, with the appropriate cosine-weighted angular distribution about the surface normal. For the IS component, some further assumptions are required about the angular and velocity distributions of the scattered OH products. As in our previous work,[44] we select these to mimic the known distributions in the molecular beam scattering experiments of Minton and coworkers on $O(^3P)$ with squalane.[58−61] For either TD or IS, if the OH trajectory traverses the probe laser beam volume it makes a contribution to the signal during the time that it is present. We accumulate these suitably weighted contributions for a sufficiently large number of trajectories to achieve satisfactory statistics on the predicted profiles. To illustrate the relationship between appearance time and OH speed, we have indicated in Figure 8b the average speeds of the TD component predicted by the MC simulations. Those for IS are similar, but not identical, because there are differences in the distributions of trajectories for the two components, with again for IS some dependence on the assumed product angular distribution.

For the TD profiles, there are slight differences between SAM and liquid samples due to the different dimensions of the active areas of the two surface types. Regardless of these minor differences, it is very obvious that in neither case is the thermal simulation a good description of the observed appearance profile. The predicted peak is significantly too late, and the observed fastest molecules at the sharply rising edge are completely missing from the simulation. We can conclude safely from this that a substantial component of the observed OH is not the result of a limiting trapping desorption mechanism.

In contrast, the IS predictions much more successfully reproduce the rapid rising edge of the experimental profiles, with more realistic peak arrival times. However, for both the SAM and liquid samples, the IS predictions decay more rapidly than the observed profiles, suggesting they are missing a slower component. Furthermore, this discrepancy is obviously somewhat greater for the slightly broader profile from squalane. If this difference is indeed real, it has an appealing mechanistic explanation. On the basis of MD simulations,[37,45,49] the squalane surface is expected to be microscopically rougher than the well-ordered outer layer of the SAM. This roughness should help to promote secondary collisions of the nascent OH and hence enhance translational energy transfer to the surface.

It is possible to go further and generate weighted sums of direct and thermal components that best match the observed profiles, which is the origin of the weightings used in Figure 8. In both cases, the direct component dominates. In terms of peak-normalized profiles, the best ratios are approximately 80:20 for the SAM and 70:30 for squalane. However, this should not be taken to be a direct measure of the relative contributions, for both the simple reason that normalized fluxes should be compared (which would be relatively straightforward) and the much less certain issue of the experimental relative detection sensitivities for the two components. Our simulations suggest that we are significantly biased in favor of the isotropic TD component, because the more nearly specular scattering of the IS component tends to lead to OH formed from $O(^3P)$ with a velocity component normal to the laser-beam axis failing to re-enter the probed volume.

Some caution should therefore clearly be exercised in any quantitative interpretation of the apparent contributions of IS and TD components. In any case, the weighted simulations are not a perfect reproduction of the observed profiles. There are a number of possible reasons for this, among which the most fundamental is that the binary separation into single-collision, impulsive events and total thermal accommodation may well be an oversimplification. In their trajectory study of inelastic scattering of O atoms from SAMs,[33] Hase and co-workers identified at least three distinct trajectory types, which they denoted direct scattering, physisorption on the top of the H-SAM, and penetration into the H-SAM layer. They have also stressed that the component of the translational energy distribution that appears to be Boltzmann-like in, for example, the inelastic scattering of the kinematically similar Ne from SAM surfaces does not necessarily arise from a thermal accommodation mechanism.[31]

Finally, we consider what further mechanistic information might be contained in our measurements of rotational populations. The statistically most reliable aspect of our measurements of rotational branching should be the OH rotational temperatures in Table 1. These data show the perhaps surprising result that at the peak of the arrival profile, the OH rotational temperature is close to thermal. According to the synthesized appearance profiles in Figure 8, there should be a significant direct contribution at the relevant pump−probe delay of 8 μs. If this contribution were hotter than thermal, we would have expected to see at least slightly higher rotational temperatures at the peak. There is some reason for anticipating that it might be, based on the moderately hotter than thermal rotational distributions that are characteristic of the related gas-phase reactions.[80,86] Our previous, more extended measurements for the reaction with squalane were indeed consistent with higher rotational temperatures for the faster-moving direct component, moderated toward the surface temperature by the increased contribution from slower, rotationally thermalized molecules at progressively later times. The slightly higher rotational temperature for OD from the C_6D_{13}−SAM in Table 1 would apparently fit this picture, but admittedly on the basis of fewer measurements than for OH with larger associated error bars. (Previous gas-phase work[87] suggests that very similar temperatures should be expected for the direct reactions of $O(^3P)$ with normal and perdeuterohydrocarbons.) Any evidence that this does also apply to the normal hydrogen SAMs is currently restricted to possible subtle differences between the $Q_1(1)$ and $R_1(5)$ profiles in Figure 7, where an earlier peak for $N' = 5$ would be consistent with a higher relative temperature of the faster moving components.

However, it is also possible that the direct reaction with SAMs really does, for some dynamical reason, produce rotationally colder OH than for squalane or the gas-phase hydrocarbons. Although this should certainly be regarded with suitable caution

given the quite limited data available so far, it is possible to speculate on rational explanations. It could conceivably be the result of an entrance-channel effect. The distinct, ordered structure of the SAM surface could restrict the geometries through which the O atom reacts with H−C bonds more than in the near random arrangement of surface groups in squalane, resulting directly in lower rotational energy release in the OH.

Perhaps more likely, the OH rotational temperatures may be an indirect signature of postreaction fates for the OH formed on SAMs and squalane. As we have argued above, a significant fraction of the O atoms must penetrate the SAM surface to at least the depth of the secondary hydrogens. This would be consistent with more of the "direct" OH products from SAMs suffering at least one secondary collision within the outer regions of the interchain channels. These restricted encounters would cause some, but incomplete, moderation of rotational and translational energies. This suggestion is consistent with the trajectory simulations of inelastic scattering by Hase and co-workers, where some of the O atoms that penetrate the SAM surface nevertheless escape with superthermal velocities. In contrast, the more open structure of squalane exposes some of the more-reactive secondary and tertiary sites to direct attack, with a higher probability of subsequent direct escape with no moderation of the nascent rotational distribution. This argument need not be inconsistent with a higher proportion of fully translationally thermalizd OH from squalane than from SAMs, as concluded above from the analysis of Figure 8. The more open structure of squalane may also allow a higher probability of ultimate escape after more than only a few secondary encounters. In contrast, those OH molecules that are formed deeper in the interchain channels of the SAM, or recoil forward to reach there, could reasonably be expected to suffer a relatively high number of secondary encounters and react to form H_2O, suppressing the apparent TD fraction.

Similar speculative arguments can be developed in an attempt to explain the apparent differences in rotational temperatures for OH and OD from SAMs. For example, if the efficiency of secondary rotational energy loss were to be higher for the lighter OH rotor than for OD, then a high probability of at least some secondary collisions for the "direct" products from SAMs would result in differential moderation of the OH and OD rotational temperatures.

It is even possible that more exotic mechanisms operate for SAMs, such as "directed ejection" proposed[15] for a component of Xe scattering from related decanethiol SAMs. This could generate OH molecules that acquire superthermal speeds, and unknown rotational distributions, having first been rotationally thermalized before being expelled repulsively from the channels between alkyl chains. Clearly, it is not possible to distinguish between the various possibilities on the basis of the current results. Further experimental work on SAMs of the type we have carried out previously for squalane to characterize rotational temperatures more fully as a function of appearance time,[46] or of surface temperature,[48] would therefore certainly be useful to begin to resolve these questions.

Nevertheless, regardless of detailed mechanistic explanations, our current results show no evidence for anything other than moderate levels of OH rotational excitation from reaction at the surface of the SAM. We can again compare this with what has been predicted theoretically. In the preliminary trajectory study of Hase and co-workers,[30] the average energy released to rotation varied with collision energy, but was in all cases slightly larger than the thermal energy at the surface temperature. The detailed rotational distributions were bimodal, mirroring the translational energy distributions. The lowest collision energy for which they report the rotational distribution is 21 kJ mol^{-1}, which should be the most relevant to our conditions. Compared to our experiments, the peak is at somewhat too high a value of N' (or J'). Troya and Schatz[39] also find bimodal rotational energy distributions, once again complementing their bimodal translation distributions. As expected, the degree of translational and rotational excitation was anticorrelated with the depth of penetration into the surface, with more deeply buried trajectories leading to energy transfer (and reaction to produce H_2O) through secondary and further multiple collisions. However, the directly scattered component was predicted to be rotationally hotter, in this case quite substantially, than we observe experimentally. This enhanced rotational excitation could simply be the result of their much higher collision energy of 5 eV, greatly exceeding the ~0.16 eV average in the current work, but this seems unlikely to be fully responsible. As noted by the authors, it may be a limitation of their relatively simple MSINDO potential surface. They had identified similar discrepancies in the corresponding low energy gas-phase reactions[88,89] and also in subsequent work on the reaction with liquid squalane.[37] This suggests that the reactions of $O(^3P)$ with SAMs, and between reactive gas-phase fragments and soft condensed phases generally, might represent a potentially fruitful area for further theoretical work to complement the new types of experiments that we have reported here.

Conclusions

We have demonstrated a viable experimental method for studying the dynamics of the reactions of $O(^3P)$ atoms with organized alkylthiol SAM layers. The relatively high reactivity, comparable to that of liquid squalane, suggests that the O atoms must be able to penetrate the SAM layer sufficiently to access the more reactive secondary hydrogens. This appears to be equally true of C_6H_{13} and $C_{18}H_{37}$−SAMs.

On the basis of the appearance profiles, the OH $v' = 0$ products are definitely not all translationally thermalized for SAMs (nor for squalane, as found previously). They must both contain a significant proportion of direct scattering. Less certainly, but with a reasonable degree of confidence, both profiles also have a slower component, consistent with thermal desorption. This component appears larger for squalane than for SAMs. If so, this would be compatible with the squalane surface being microscopically rougher than the SAMs, enhancing translational energy loss in secondary collisions of the escaping OH.

Our measured rotational distributions at the peak of the OH appearance profile currently indicate modest rotational excitation of the direct products. Further work is required to fully characterize any correlations between OH product velocity and rotational temperature.

Accurate theoretical predictions against which to compare these new results are currently limited, and we suggest this as a potentially fruitful area for further theoretical modeling.

Acknowledgment. We thank Dr Manfred Buck, University of St. Andrews for making available STM equipment and advice on SAM preparation. We are grateful to Dr. Ron Brown, University of Edinburgh, for assistance with the collection of XPS data. MLC is supported by an RCUK Academic Fellowship. We acknowledge a research grant from EPSRC.

Supporting Information Available: XPS spectra of C_6H_{13}−SAMs as prepared from solution, having been in vacuum at base pressure for a prolonged period, and following NO_2

exposure for 1 h, respectively. The spectra show the obvious alteration of the SAMs composition following extended NO_2 exposure. This information is available free of charge via the Internet at http://pubs.acs.org.

References and Notes

(1) Love, J. C.; Estroff, L. A.; Kriebel, J. K.; Nuzzo, R. G.; Whitesides, G. M. *Chem. Rev.* **2005**, *105*, 1103.
(2) Schreiber, F. *Prog. Surf. Sci.* **2000**, *65*, 151.
(3) Paz, Y.; Trakhtenberg, S.; Naaman, R. *J. Phys. Chem.* **1992**, *96*, 10964.
(4) Paz, Y.; Trakhtenberg, S.; Naaman, R. *J. Phys. Chem.* **1994**, *98*, 13517.
(5) Qin, X.; Tzvetkov, T.; Jacobs, D. C. *Nucl. Instrum. Methods Phys. Res., Sect. B* **2003**, *203*, 130.
(6) Qin, X. D.; Tzvetkov, T.; Liu, X.; Lee, D. C.; Yu, L. P.; Jacobs, D. C. *J. Am. Chem. Soc.* **2004**, *126*, 13232.
(7) Qin, X. D.; Tzvetkov, T.; Jacobs, D. C. *J. Phys. Chem. A* **2006**, *110*, 1408.
(8) Torres, J.; Perry, C. C.; Bransfield, S. J.; Fairbrother, D. H. *J. Phys. Chem. B* **2002**, *106*, 6265.
(9) Wagner, A. J.; Wolfe, G. M.; Fairbrother, D. H. *J. Chem. Phys.* **2004**, *120*, 3799.
(10) Cohen, S. R.; Naaman, R.; Sagiv, J. *Phys. Rev. Lett.* **1987**, *58*, 1208.
(11) Gibson, K. D.; Isa, N.; Sibener, S. J. *J. Chem. Phys.* **2003**, *119*, 13083.
(12) Darling, S. B.; Rosenbaum, A. M.; Sibener, S. J. *Surf. Sci.* **2001**, *478*, L313.
(13) Yan, T. Y.; Isa, N.; Gibson, K. D.; Sibener, S. J.; Hase, W. L. *J. Phys. Chem. A* **2003**, *107*, 10600.
(14) Isa, N.; Gibson, K. D.; Yan, T.; Hase, W.; Sibener, S. J. *J. Chem. Phys.* **2004**, *120*, 2417.
(15) Gibson, K. D.; Isa, N.; Sibener, S. J. *J. Phys. Chem. A* **2006**, *110*, 1469.
(16) Day, B. S.; Davis, G. M.; Morris, J. R. *Anal. Chim. Acta* **2003**, *496*, 249.
(17) Day, B. S.; Morris, J. R. *J. Phys. Chem. B* **2003**, *107*, 7120.
(18) Day, B. S.; Shuler, S. F.; Ducre, A.; Morris, J. R. *J. Chem. Phys.* **2003**, *119*, 8084.
(19) Day, B. S.; Morris, J. R.; Troya, D. *J. Chem. Phys.* **2005**, *122*, 214712.
(20) Day, B. S.; Morris, J. R. *J. Chem. Phys.* **2005**, *122*, 234714.
(21) Lohr, J. R.; Day, B. S.; Morris, J. R. *J. Phys. Chem. B* **2005**, *109*, 15469.
(22) Day, B. S.; Morris, J. R.; Alexander, W. A.; Troya, D. *J. Phys. Chem. A* **2006**, *110*, 1319.
(23) Lohr, J. R.; Day, B. S.; Morris, J. R. *J. Phys. Chem. A* **2006**, *110*, 1645.
(24) Vazquez, S. A.; Morris, J. R.; Rahaman, A.; Mazyar, O. A.; Vayner, G.; Addepalli, S. V.; Hase, W. L.; Martinez-Nunez, E. *J. Phys. Chem. A* **2007**, *111*, 12785.
(25) Alexander, W. A.; Day, B. S.; Moore, H. J.; Lee, T. R.; Morris, J. R.; Troya, D. *J. Chem. Phys.* **2008**, *128*, 014713.
(26) Tasic, U.; Day, B. S.; Yan, T. Y.; Morris, J. R.; Hase, W. L. *J. Phys. Chem. C* **2008**, *112*, 476.
(27) Saecker, M. E.; Govoni, S. T.; Kowalski, D. V.; King, M. E.; Nathanson, G. M. *Science* **1991**, *252*, 1421.
(28) Nathanson, G. M. *Annu. Rev. Phys. Chem.* **2004**, *55*, 231.
(29) Yan, T. Y.; Hase, W. L.; Barker, J. R. *Chem. Phys. Lett.* **2000**, *329*, 84.
(30) Li, G.; Bosio, S. B. M.; Hase, W. L. *J. Mol. Struct.* **2000**, *556*, 43.
(31) Yan, T. Y.; Hase, W. L. *J. Phys. Chem. B* **2002**, *106*, 8029.
(32) Yan, T. Y.; Hase, W. L.; Tully, J. C. *J. Chem. Phys.* **2004**, *120*, 1031.
(33) Tasic, U. S.; Yan, T. Y.; Hase, W. L. *J. Phys. Chem. B* **2006**, *110*, 11863.
(34) Martinez-Nunez, E.; Rahaman, A.; Hase, W. L. *J. Phys. Chem. C* **2007**, *111*, 354.
(35) Garton, D. J.; Brunsvold, A. L.; Minton, T. K.; Troya, D.; Maiti, B.; Schatz, G. C. *J. Phys. Chem. A* **2006**, *110*, 1327.
(36) Tasic, U.; Troya, D. *Phys. Chem. Chem. Phys.* **2008**, *10*, 5776.
(37) Kim, D.; Schatz, G. C. *JJ. Phys. Chem. A* **2007**, *111*, 5019.
(38) Chase, D.; Manning, M.; Morgan, J. A.; Nathanson, G. M.; Gerber, R. B. *J. Chem. Phys.* **2000**, *113*, 9279.
(39) Troya, D.; Schatz, G. C. *J. Chem. Phys.* **2004**, *120*, 7696.
(40) Leger, L. J.; Visentine, J. T. *Aerosp. Am.* **1986**, *24*, 32.
(41) Leger, L. J.; Visentine, J. T. *J. Spacecraft Rockets* **1986**, *23*, 505.
(42) Murr, L. E.; Kinard, W. H. *Am. Sci.* **1993**, *81*, 152.
(43) Kelso, H.; Kohler, S. P. K.; Henderson, D. A.; McKendrick, K. G. *J. Chem. Phys.* **2003**, *119*, 9985.
(44) Kohler, S. P. K.; Allan, M.; Kelso, H.; Henderson, D. A.; McKendrick, K. G. *J. Chem. Phys.* **2005**, *122*, 024712.
(45) Kohler, S. P. K.; Reed, S. K.; Westacott, R. E.; McKendrick, K. G. *J. Phys. Chem. B* **2006**, *110*, 11717.
(46) Kohler, S. P. K.; Allan, M.; Costen, M. L.; McKendrick, K. G. *J. Phys. Chem. B* **2006**, *110*, 2771.
(47) Allan, M.; Bagot, P. A. J.; Kohler, S. P. K.; Reed, S. K.; Westacott, R. E.; Costen, M. L.; McKendrick, K. G. *Phys. Scr.* **2007**, *76*, C42.
(48) Allan, M.; Bagot, P. A. J.; Costen, M. L.; McKendrick, K. G. *J. Phys. Chem. C* **2007**, *111*, 14833.
(49) Allan, M.; Bagot, P. A. J.; Westacott, R. E.; Costen, M. L.; McKendrick, K. G. *J. Phys. Chem. C* **2008**, *112*, 1524.
(50) Kenyon, A. J.; McCaffery, A. J.; Quintella, C. M.; Zidan, M. D. *Chem. Phys. Lett.* **1992**, *190*, 55.
(51) Kenyon, A. J.; McCaffery, A. J.; Quintella, C. M.; Zidan, M. D. *Faraday Discuss.* **1993**, *96*, 245.
(52) Kenyon, A. J.; McCaffery, A. J.; Quintella, C. M.; Zidan, M. D. *J. Chem. Soc., Faraday Trans.* **1993**, *89*, 3877.
(53) Perkins, B. G.; Haber, T.; Nesbitt, D. J. *J. Phys. Chem. B* **2005**, *109*, 16396.
(54) Perkins, B. G.; Nesbitt, D. J. *J. Phys. Chem. B* **2006**, *110*, 17126.
(55) Perkins, B. G.; Nesbitt, D. J. *J. Phys. Chem. A* **2007**, *111*, 7420.
(56) Perkins, B. G.; Nesbitt, D. J. *J. Phys. Chem. B* **2008**, *112*, 507.
(57) Zolot, A. M.; Harper, W. W.; Perkins, B. G.; Dagdigian, P. J.; Nesbitt, D. J. *J. Chem. Phys.* **2006**, *125*, 021101.
(58) Garton, D. J.; Minton, T. K.; Alagia, M.; Balucani, N.; Casavecchia, P.; Volpi, G. G. *J. Chem. Phys.* **2000**, *112*, 5975.
(59) Minton, T. K.; Seale, J. W.; Garton, D. J.; Frandsen, A. K. *Prot. Space Mater. Space Environ.* **2001**, *4*, 15.
(60) Zhang, J. M.; Garton, D. J.; Minton, T. K. *J. Chem. Phys.* **2002**, *117*, 6239.
(61) Zhang, J. M.; Upadhyaya, H. P.; Brunsvold, A. L.; Minton, T. K. *J. Phys. Chem. B* **2006**, *110*, 12500.
(62) Bagot, P. A. J.; Waring, C.; Costen, M. L.; McKendrick, K. G. *J. Phys. Chem. C* **2008**, *112*, 10868.
(63) Harris, J. G. *J. Phys. Chem.* **1992**, *96*, 5077.
(64) Martin, M. G.; Siepmann, J. I. *J. Phys. Chem. B* **1999**, *103*, 4508.
(65) Wick, C. D.; Siepmann, J. I.; Schure, M. R. *Anal. Chem.* **2002**, *74*, 3518.
(66) Xie, B. Q.; Shi, H. F.; Jiang, S. C.; Zhao, Y.; Han, C. C.; Xu, D. F.; Wang, D. J. *J. Phys. Chem. B* **2006**, *110*, 14279.
(67) Wang, S. L.; Tozaki, K.; Hayashi, H.; Hosaka, S.; Inaba, H. *Thermochim. Acta* **2003**, *408*, 31.
(68) Wang, S. L.; Tozaki, K. I.; Hayashi, H.; Inaba, H.; Yamamoto, H. *Thermochim. Acta* **2006**, *448*, 73.
(69) Taggart, A. M.; Voogt, F.; Clydesdale, G.; Roberts, K. J. *Langmuir* **1996**, *12*, 5722.
(70) Sefler, G. A.; Du, Q.; Miranda, P. B.; Shen, Y. R. *Chem. Phys. Lett.* **1995**, *235*, 347.
(71) Pfohl, T.; Beaglehole, D.; Riegler, H. *Chem. Phys. Lett.* **1996**, *260*, 82.
(72) Wu, X. Z.; Sirota, E. B.; Sinha, S. K.; Ocko, B. M.; Deutsch, M. *Phys. Rev. Lett.* **1993**, *70*, 958.
(73) Ocko, B. M.; Wu, X. Z.; Sirota, E. B.; Sinha, S. K.; Gang, O.; Deutsch, M. *Phys. Rev. E* **1997**, *55*, 3164.
(74) Esenturk, O.; Walker, R. A. *J. Chem. Phys.* **2006**, *125*, 174701.
(75) Kawamata, M.; Yamamoto, T. *J. Phys. Soc. Jpn.* **1997**, *66*, 2350.
(76) Shimizu, T.; Yamamoto, T. *J. Chem. Phys.* **2000**, *113*, 3351.
(77) Li, H. Z.; Yamamoto, T. *J. Chem. Phys.* **2001**, *114*, 5774.
(78) Baker, R. P.; Costen, M. L.; Hancock, G.; Ritchie, G. A. D.; Summerdeld, D. *Phys. Chem. Chem. Phys.* **2000**, *2*, 661.
(79) Troya, D. *J. Phys. Chem. A* **2007**, *111*, 10745.
(80) Ausfelder, F.; McKendrick, K. G. *Prog. React. Kinet. Mech.* **2000**, *25*, 299.
(81) Willey, T. M.; Vance, A. L.; van Buuren, T.; Bostedt, C.; Terminello, L. J.; Fadley, C. S. *Surf. Sci.* **2005**, *576*, 188.
(82) Schoenfisch, M. H.; Pemberton, J. E. *J. Am. Chem. Soc.* **1998**, *120*, 4502.
(83) Bucher, J. P.; Santesson, L.; Kern, K. *Langmuir* **1994**, *10*, 979.
(84) Kondoh, H.; Kodama, C.; Sumida, H.; Nozoye, H. *J. Chem. Phys.* **1999**, *111*, 1175.
(85) Bain, C. D.; Troughton, E. B.; Tao, Y. T.; Evall, J.; Whitesides, G. M.; Nuzzo, R. G. *J. Am. Chem. Soc.* **1989**, *111*, 321.
(86) Sweeney, G. M.; Watson, A.; McKendrick, K. G. *J. Chem. Phys.* **1997**, *106*, 9172.
(87) Ausfelder, F.; Kelso, H.; McKendrick, K. G. *Phys. Chem. Chem. Phys.* **2002**, *4*, 473.
(88) Troya, D.; Pascual, R. Z.; Schatz, G. C. *J. Phys. Chem. A* **2003**, *107*, 10497.
(89) Troya, D.; Pascual, R. Z.; Garton, D. J.; Minton, T. K.; Schatz, G. C. *J. Phys. Chem. A* **2003**, *107*, 7161.

JP8109868